PERGAMON

International Journal of Solids and Structures 38 (2001) 635–656

INTERNATIONAL JOURNAL OF SOLIDS and STRUCTURES

www.elsevier.com/locate/ijsolstr

Numerical analysis and large strain elastic–viscoplastic behavior of hydrostatic stress-sensitive metals

Michael Brünig *

Lehrstuhl für Baumechanik-Statik, Universität Dortmund, August-Schmidt Strasse 8, D-44221 Dortmund, Germany

Received 11 May 1999; in revised form 8 March 2000

Abstract

The paper deals with the numerical simulation of the elastic–viscoplastic deformation and localization behavior of metals. The model is based on a generalized macroscopic theory taking into account sensitivity to hydrostatic stress and irreversible dilatant deformation behavior observed in experiments. Hence, particular attention is focused on the introduction of an equivalent stress measure which is based on a generalized I_1–J_2 criterion to be able to simulate numerically the effect of hydrostatic stress on the viscoplastic flow properties of metals. Corresponding computational aspects are discussed in some detail. Finite element analyses of large strain elastic-rate-dependent plastic problems involving severe localization will be presented, and the influence of various model parameters on the deformation and localization behavior will be discussed.

Keywords: Hydrostatic stress-sensitive metals; Viscoplasticity; Large strains; Finite element analyses; Localization

1. Introduction

Numerical simulations of large strain inelastic problems have emerged as a crucial part of the industrial design with a wide variety of applications involving complex constitutive models. Numerous technical papers have been published tackling a broad range of theoretical issues to model and to predict the macroscopic finite inelastic deformation behavior of polycrystalline metals undergoing complex loading conditions.

The key aspects of any constitutive model are its ability to reproduce the behavior of engineering materials and the cost of its algorithmic implementation which opens the possibility of numerical simulations. In particular, the broad general scope of the constitutitve model may come at the expense of precision in specific circumstances. Thus, there is an inevitable trade-off between the generality of the mathematical material model taking into account a large number of experimental observations and its accuracy in special applications. Looking, for example, at some of the available viscoplastic theories discussed in the literature

* Tel.: +49-231-755-4682; fax: +49-231-755-2532.
E-mail address: bruenig@busch.bauwesen.uni-dortmund.de (M. Brünig).

0020-7683/01/$ - see front matter
PII: S0020-7683(00)00092-5

(Perzyna, 1966), it seems that the efforts to create constitutive models showing the appropriate response in simulation of experimentally observed material behavior are often at the expense of the algorithmic implementation and, hence, limit the possible final computational application of these models. Therefore, there are always trade-offs between realism in the simulated behavior and manageability of the governing equations using them in a finite element program. Thus, the validity of a material model can only be judged by the simultaneous satisfaction of the four mean aspects of generality and accuracy as well as realism and manageability. The philosophy underlying the appropriate finite strain material model may be that physical mechanisms can be seen as the key to the best solution. Hence, the macroscopic constitutive model should be based on the same metallurgical events which cause the microscopic deformations in the material to come closest to simultaneous satisfaction of all the four aspects stated above.

As discussed, for example, by Hill (1950) and Khan and Huang (1995), macroscopically based inelastic continuum approaches are chosen in a large number of engineering applications. The main problem of macroscopic theories of plasticity is to establish appropriate constitutive relations and evolution equations. They start from experimental observations and elementary mechanical assumptions concerning the deformation behavior. The overall macroscopic response of the solid is then obtained from sound phenomenological models which rely on micromechanical considerations. In particular, rate-independent and rate-dependent constitutive models are discussed in plasticity literature which are based on experimental results and numerical simulations in metal physics. Then, after identifying the relevant physical mechanisms appropriate constitutive equations have to be formulated. Clearly, the most direct approach would be to mathematically model each mechanism based on the best available fundamental research, and then to combine them all into a set of governing equations. But it has been shown that with respect to engineering materials many fine details of the internal structure do not strongly influence their global behavior and, therefore, most idealized engineering models rely on macroscopic phenomenology.

Experimental results obtained from simple uniaxial tension and compression tests with polycrystalline metal specimens tend to confirm isochoric theories and plastically non-dilatant flow rules, but experimental studies on the effect of superimposed hydrostatic pressure on the deformation behavior of iron based materials (Spitzig et al., 1975, 1976) have shown that the flow stress depends approximately linearly on hydrostatic pressure. These tests also indicate that plastic deformations may be accompanied by a permanent volume expansion.

These effects are generally ignored in computational metal viscoplasticity but previous finite element analyses on the effect of superimposed hydrostatic stress on the finite elastic–plastic deformation behavior of crystalline solids have been presented by Brünig (1997, 1998) and Brünig and Obrecht (1998). Their rate-independent formulations take into account deviations from the classical Schmid-rule of the critical resolved shear stress in the microscale as well as microscopic plastic volume changes including a macroscopic non-associated flow rule. Preliminary numerical simulations demonstrate the influence of additional constitutive and kinematic parameters on plastic yielding and permanent volume expansion in tension and compression tests. In addition, Brünig (1999c) presented a large strain elastic-rate-independent plastic macroscopic model taking into account the hydrostatic stress sensitivity of metals. His numerical studies have shown that even small additional parameters remarkably affect the onset of localization as well as the associated deformation modes, and that they can lead to a notable decrease in ductility.

Furthermore, in phenomenological plasticity literature, it has long been recognized that the notion of rate-independence of plastic response is only a convenient approximation at low homologous temperatures. But plastic flow due to dislocation motion may be inherently rate-dependent even at low temperatures. For example, studies on micromechanical behavior of polycrystalline metals have shown that macroscopic inelastic deformations are a consequence of motion of dislocations and similar microscopic defects. Even at small strain levels and moderate homologous temperatures, dislocations migrate thus giving rise to small inelastic strains. Therefore, rate-dependent plasticity theories dealing with the finite deformation behavior of metals become more and more important even in moderate temperature applications.

The present constitutive model is an unified approach in which a single strain rate equation generates all of the inelastic strain behavior and no separate assumptions are employed for rate-dependent plasticity and creep. All inelastic deformations are considered to be rate-dependent. Appropriate formulations presented in literature are based on the separation of the total deformation rate into geometrically reversible (elastic) and irreversible (inelastic) parts. Due to its strong physical basis, Rice (1970, 1971) and Anand (1985) have chosen internal state variable formulations as an appropriate basis in formulating rate-dependent constitutive equations. Within this rate-dependent model, viscoplastic flow is assumed to occur at all nonzero values of stress, although at low stress levels the rate of viscoplastic flow may be immeasurably small. Therefore, the theory requires neither yield condition nor loading and unloading criteria. The equivalent viscoplastic strain rate, which is typically determined by the consistency condition in rate-independent plasticity models, needs to be prescribed by an appropriate constitutive function. Hence, the overall mathematical structure of this rate-dependent model is simple because the viscoplastic flow rule is a smooth function in stress space. In addition, in rate-dependent plasticity theories, the inelastic strains are functions of internal state variables and current deformation at all stages of loading and unloading. These internal state variables take into account the current structural arrangement at the microscale. Since microscopic dislocations play a principal role in the production of inelastic macroscopic strains, the internal state variables employed in the phenomenological material model should specify the dislocation distribution in some detail. However, appropriate internal variables and their rate evolution equations are generally not easily identifiable. The accurate assessment of inelastic strains calculated by appropriate viscoplastic models, on the other hand, is an essential input for life prediction methods which may lead to more accurate determination of the service life of structural components.

Thus, the present paper deals with the numerical simulation of the elastic–viscoplastic deformation and localization behavior of metals which are viscoplastically dilatant and sensitive to hydrostatic stress. The continuum formulation starts from a multiplicative decomposition of the mixed-variant metric transformation tensor into elastic and viscoplastic parts. This leads to the definition of an appropriate logarithmic strain measure whose rate is shown to be additively decomposed into elastic and viscoplastic terms. The mixed-variant logarithmic elastic strain tensor is employed to define an isotropic hyperelastic constitutive relation which leads to a generalized Hooke law for large strain analyses. Particular attention is focused on the introduction of an equivalent stress measure which takes into account the resistance to viscoplastic flow. It is based on a generalized I_1–J_2 criterion to be able to simulate numerically the effect of hydrostatic stress on the viscoplastic flow properties in metals. The viscoplastic part of the logarithmic strain rate tensor is chosen to be a function of the current stress state and an equivalent viscoplastic strain rate which will be prescribed by an appropriate constitutive function. Corresponding computational aspects will be discussed in some detail. Finally, numerical simulations of the elastic-rate-dependent plastic deformation behavior of viscoplastically dilatant and hydrostatic stress-sensitive metals will demonstrate the efficiency of the formulation and the algorithm. Large strain problems involving severe localization phenomena will be presented to discuss the influence of various model parameters on the deformation and load-carrying behavior of rate-dependent hydrostatic stress-sensitive metals.

2. Fundamental governing equations

The large strain elastic–viscoplastic theory is based on the introduction of the mixed-variant metric transformation tensor introduced by Lehmann (1982a,b) which will be multiplicatively decomposed into a viscoplastic and an elastic part and lead to the definition of appropriate logarithmic strain measures. This framework, which has also been used by Brünig (1999a,b,c), avoids a priori the introduction of inelastic rotations which are controversially discussed in the literature. Thus, it stands in contrast to mechanical formulations based on the multiplicative decomposition of the deformation gradient into a (visco) plastic

and an elastic part proposed by Lee (1969) which has been used, for example, by Weber and Anand (1990), Eterovic and Bathe (1990), Perić et al. (1992), and Sansour and Kollmann (1997) to develop material models for finite deformation theories taking into account logarithmic strain tensors.

In particular, the kinematic theory for the mechanics of large deformations of solids is based on the metric transformation tensor

$$\mathbf{Q} = Q^{i}_{\cdot j}\mathring{\mathbf{g}}_i \otimes \mathring{\mathbf{g}}^j = \mathring{G}^{ik} G_{kj}\mathring{\mathbf{g}}_i \otimes \mathring{\mathbf{g}}^j = \mathring{\mathbf{G}}^{-1}\mathbf{C}. \tag{1}$$

In Eq. (1), $\mathring{\mathbf{g}}_i$ and $\mathring{\mathbf{g}}^j$ denote the covariant and contravariant base vectors of the initial configuration, respectively, G_{ij} and $\mathring{G}_{ij}$ represent the metric coefficients of the base vectors with respect to the current and initial configurations, and $\mathbf{C}$ and $\mathring{\mathbf{G}}$ are the associated tensors with respect to the undeformed initial configuration. This leads to the definition of the mixed-variant logarithmic Hencky strain tensor:

$$\mathbf{H} = \tfrac{1}{2}\ln\mathbf{Q} = \tfrac{1}{2}(\ln Q)^{i}_{\cdot j}\mathring{\mathbf{g}}_i \otimes \mathring{\mathbf{g}}^j = H^{i}_{\cdot j}\mathring{\mathbf{g}}_i \otimes \mathring{\mathbf{g}}^j. \tag{2}$$

The spherical part of the logarithmic strain tensor,

$$\operatorname{tr}\mathbf{H} = \mathbf{H}\cdot\mathbf{1} = \ln\frac{\mathrm{d}v}{\mathrm{d}v_0} = \ln J, \tag{3}$$

exactly describes the volume change of the solid and, thus, corresponds to the logarithm of $J = \sqrt{\det\mathbf{C}}$. Then, the deviatoric part of the Hencky strain tensor,

$$\operatorname{dev}\mathbf{H} = \mathbf{H} - \tfrac{1}{3}\operatorname{tr}\mathbf{H}\mathbf{1}, \tag{4}$$

represents isochoric deformations.

Following the fundamental ideas of Lehmann (1982a,b), the macroscopic formulation of the large deformation behavior of elastic–viscoplastic materials is based on the multiplicative decomposition of the metric transformation tensor $\mathbf{Q}$ into its respective rate-dependent plastic and elastic parts:

$$\mathbf{Q} = \mathbf{Q}^{\mathrm{vp}}\mathbf{Q}^{\mathrm{el}} \tag{5}$$

with

$$\mathbf{Q}^{\mathrm{vp}} = \mathring{G}^{ik}\overset{*}{G}_{kj}\mathring{\mathbf{g}}_i \otimes \mathring{\mathbf{g}}^j, \tag{6}$$

$$\mathbf{Q}^{\mathrm{el}} = \overset{*}{G}^{ik} G_{kj}\mathring{\mathbf{g}}_i \otimes \mathring{\mathbf{g}}^j. \tag{7}$$

In Eqs. (6) and (7), $\overset{*}{G}_{ij}$ denotes the metric tensor of the base vectors of an intermediate configuration which represents a fictitious unstressed state at fixed values of the internal variables. To describe reversible deformations, the elastic strain tensor,

$$\mathbf{H}^{\mathrm{el}} = \tfrac{1}{2}\ln\mathbf{Q}^{\mathrm{el}}, \tag{8}$$

is introduced. These strains are assumed to be kinematically independent from accompanying inelastic deformations. Furthermore, the strain rate tensors

$$\dot{\mathbf{H}} = \tfrac{1}{2}\mathbf{Q}^{-1}\dot{\mathbf{Q}}, \tag{9}$$

$$\dot{\mathbf{H}}^{\mathrm{el}} = \tfrac{1}{2}\mathbf{Q}^{\mathrm{el}-1}\dot{\mathbf{Q}}^{\mathrm{el}} \tag{10}$$

are considered. Taking account of the multiplicative decomposition (5), Eq. (9) leads to the additive decomposition of the total strain rate,

$$\dot{\mathbf{H}} = \tfrac{1}{2}\mathbf{Q}^{\mathrm{el}-1}\mathbf{Q}^{\mathrm{vp}-1}\dot{\mathbf{Q}}^{\mathrm{vp}}\mathbf{Q}^{\mathrm{el}} + \tfrac{1}{2}\mathbf{Q}^{\mathrm{el}-1}\dot{\mathbf{Q}}^{\mathrm{el}} = \dot{\mathbf{H}}^{\mathrm{vp}} + \dot{\mathbf{H}}^{\mathrm{el}}, \tag{11}$$

into its elastic (10) and viscoplastic parts using the definition,

$$\dot{\mathbf{H}}^{\mathrm{vp}} = \tfrac{1}{2}\mathbf{Q}^{-1}\dot{\mathbf{Q}}^{\mathrm{vp}}\mathbf{Q}^{\mathrm{el}}, \tag{12}$$

which will be employed to formulate the inelastic constitutive behavior.

Now, using the strain rate tensor $\dot{\mathbf{H}}$ and its work-conjugate counterpart, the mixed-variant stress tensor,

$$\mathbf{T} = T^{i}_{\ .j}\mathring{\mathbf{g}}_i \otimes \mathring{\mathbf{g}}^j, \tag{13}$$

the rate of specific mechanical work $\dot{w}$ is given by

$$\rho_0\dot{w} = \mathbf{T}\cdot\dot{\mathbf{H}}, \tag{14}$$

where ρ_0 denotes the initial mass density. The rate of mechanical work (14) can be additively decomposed according to

$$\rho_0\dot{w} = \rho_0\dot{w}^{\mathrm{el}} + \rho_0\dot{w}^{\mathrm{vp}} = \mathbf{T}\cdot\dot{\mathbf{H}}^{\mathrm{el}} + \mathbf{T}\cdot\dot{\mathbf{H}}^{\mathrm{vp}} \tag{15}$$

into an elastic part $\dot{w}^{\mathrm{el}}$ governed by thermodynamic state equations as well as into a viscoplastic part $\dot{w}^{\mathrm{vp}}$. In the present formulation, inelastic stresses which require to overcome the internal viscous mechanisms are not considered, and the total stress tensor is taken to fully correspond to the elastic strains.

Moreover, the specific free-energy function ϕ is introduced and is assumed to be additively decomposed into an elastic and a viscoplastic part,

$$\phi = \phi^{\mathrm{el}} + \phi^{\mathrm{vp}}, \tag{16}$$

which will be expressible as functions of thermodynamic state variables. Thus, the elastic part $\phi^{\mathrm{el}}(\mathbf{H}^{\mathrm{el}})$ may be formulated in terms of the elastic strain tensor, whereas the viscoplastic part ϕ^{vp} takes into account the internal state variables to carry forward informations from the microscale to the phenomenological macroscale.

In this context, the second law of thermodynamics (Clausius–Duhem inequality) for isothermal processes can be written in the form

$$\dot{w} - \dot{\phi} \geqslant 0. \tag{17}$$

Making use of Eqs. (15) and (16), one arrives at

$$\mathbf{T}\cdot\dot{\mathbf{H}}^{\mathrm{el}} + \mathbf{T}\cdot\dot{\mathbf{H}}^{\mathrm{vp}} - \rho_0\frac{\partial\phi^{\mathrm{el}}}{\partial\mathbf{H}^{\mathrm{el}}}\cdot\dot{\mathbf{H}}^{\mathrm{el}} - \rho_0\dot{\phi}^{\mathrm{vp}} \geqslant 0 \tag{18}$$

or

$$\left(\mathbf{T} - \rho_0\frac{\partial\phi^{\mathrm{el}}}{\partial\mathbf{H}^{\mathrm{el}}}\right)\cdot\dot{\mathbf{H}}^{\mathrm{el}} + \mathbf{T}\cdot\dot{\mathbf{H}}^{\mathrm{vp}} - \rho_0\dot{\phi}^{\mathrm{vp}} \geqslant 0. \tag{19}$$

Now, standard arguments concerning nondissipative processes in the isotropic elastic range lead to the potential relation for the mixed-variant stress tensor (thermic state equation),

$$\mathbf{T} = \rho_0\frac{\partial\phi^{\mathrm{el}}}{\partial\mathbf{H}^{\mathrm{el}}}, \tag{20}$$

and, assuming Eq. (20) to hold in the viscoplastic range as well, Eq. (19) reduces to the so-called intrinsic dissipation inequality,

$$D = \mathbf{T}\cdot\dot{\mathbf{H}}^{\mathrm{vp}} - \rho_0\dot{\phi}^{\mathrm{vp}} \geqslant 0, \tag{21}$$

where D represents the dissipation function. Thus, the evolution equation for the viscoplastic part of the deformation will be formulated in terms of $\dot{\mathbf{H}}^{\mathrm{vp}}$ defined by Eq. (12).

3. Constitutive equations

The finite elastic part of the isotropic material behavior is assumed to be governed by the Helmholtz free-energy function:

$$\rho_0\phi^{\mathrm{el}} = \mu\,\mathrm{dev}\,\mathbf{H}^{\mathrm{el}}\cdot\mathrm{dev}\,\mathbf{H}^{\mathrm{el}} + \tfrac{1}{2}K(\mathrm{tr}\,\mathbf{H}^{\mathrm{el}})^2, \tag{22}$$

where μ and K represent the shear and bulk modulus of the material, respectively. It admits an additive decomposition of the elastic Hencky strain tensor,

$$\mathbf{H}^{\mathrm{el}} = \mathrm{dev}\,\mathbf{H}^{\mathrm{el}} + \tfrac{1}{3}\mathrm{tr}\,\mathbf{H}^{\mathrm{el}}\mathbf{1} \tag{23}$$

into the elastic bulk strain $\mathrm{tr}\,\mathbf{H}^{\mathrm{el}}\mathbf{1}$ computing the elastic dilatation as well as the deviator $\mathrm{dev}\,\mathbf{H}^{\mathrm{el}}$ representing isochoric elastic deformations. Taking into account the hyperelastic constitutive relationship (20), the mixed-variant stress tensor may be expressed in the form:

$$\mathbf{T} = 2\mu\,\mathrm{dev}\,\mathbf{H}^{\mathrm{el}} + K\,\mathrm{tr}\,\mathbf{H}^{\mathrm{el}}\mathbf{1}. \tag{24}$$

If any effect of plastic straining on the finite elastic material behavior is neglected, the associated tensor of elastic moduli may be determined from

$$\mathbb{C} = \rho_0\frac{\partial^2\phi^{\mathrm{el}}}{\partial\mathbf{H}^{\mathrm{el}}\otimes\partial\mathbf{H}^{\mathrm{el}}} = 2\mu\mathbb{1}^D + K\,\mathbf{1}\otimes\mathbf{1} \tag{25}$$

with

$$\mathbb{1}^D = \left(\delta^i_k\delta^l_j - \tfrac{1}{3}\delta^i_j\delta^l_k\right)\mathring{\mathbf{g}}_i\otimes\mathring{\mathbf{g}}^j\otimes\mathring{\mathbf{g}}_l\otimes\mathring{\mathbf{g}}^k \tag{26}$$

and the second order identity tensor $\mathbf{1}$.

The viscoplastic deformation rate is assumed to be related to the current stress tensor through the flow rule of classical viscoplasticity theory and, therefore, satisfies the positive work dissipation requirements (21). To compute dilatant inelastic deformations, the viscoplastic potential function is given by the relation,

$$g^{\mathrm{vp}} = bI_1 + \sqrt{J_2}, \tag{27}$$

where $I_1 = \mathrm{tr}\,\mathbf{T}$ and $J_2 = \tfrac{1}{2}\mathrm{dev}\,\mathbf{T}\cdot\mathrm{dev}\,\mathbf{T}$ are invariants of the stress tensor (13), and b represents the viscoplastic dilatation coefficient. This leads to the viscoplastic flow law:

$$\dot{\mathbf{H}}^{\mathrm{vp}} = \dot{\lambda}\frac{\partial g^{\mathrm{vp}}}{\partial\mathbf{T}} = \dot{\lambda}\left(\frac{1}{2\sqrt{J_2}}\mathrm{dev}\,\mathbf{T} + b\mathbf{1}\right), \tag{28}$$

where $\dot{\lambda}$ is a nonnegative scalar-valued factor.

A principal feature of the present viscoplastic theory is the consideration that in the solid modeled by Eq. (28), there is always a viscoplastic contribution of the strain rate which depends on the current state of stress regardless of the direction of the stress rate. In particular, this hypothesis is partially motivated by the extensive work in the field of dislocation dynamics which has shown that the dislocation velocity and, therefore, the uniaxial viscoplastic strain rate is predominantly a function of the current stress state.

In addition, the deviatoric orientation tensor,

$$\mathbf{N} = \frac{1}{\sqrt{2J_2}}\mathrm{dev}\,\mathbf{T}, \tag{29}$$

is introduced which satisfies the conditions $\mathbf{N}\cdot\mathbf{N} = 1$ and $\mathbf{N}\cdot\dot{\mathbf{N}} = 0$. This leads to the definition of the isochoric equivalent viscoplastic strain rate,

$$\dot{\gamma}_{\mathrm{iso}} = \mathbf{N} \cdot \dot{\mathbf{H}}^{\mathrm{vp}} = \frac{1}{\sqrt{2}} \dot{\lambda}, \tag{30}$$

which is used to express the viscoplastic strain rate tensor (28) in the form:

$$\dot{\mathbf{H}}^{\mathrm{vp}} = \dot{\gamma}_{\mathrm{iso}} \mathbf{N} + \dot{\gamma}_{\mathrm{iso}} \sqrt{2} b \mathbf{1} = \mathrm{dev}\, \dot{\mathbf{H}}^{\mathrm{vp}} + \tfrac{1}{3} \mathrm{tr}\, \dot{\mathbf{H}}^{\mathrm{vp}} \mathbf{1}. \tag{31}$$

Thus, it is possible to identify isochoric as well as dilatant viscoplastic strain rates,

$$\mathrm{dev}\, \dot{\mathbf{H}}^{\mathrm{vp}} = \dot{\gamma}_{\mathrm{iso}} \mathbf{N} \tag{32}$$

and

$$\mathrm{tr}\, \dot{\mathbf{H}}^{\mathrm{vp}} = 3\sqrt{2} b \dot{\gamma}_{\mathrm{iso}}, \tag{33}$$

respectively.

The total equivalent viscoplastic strain rate is prescribed by an appropriate function of the form:

$$\dot{\gamma} = \dot{\gamma}(c, g), \tag{34}$$

where c represents an equivalent stress measure and g is the scalar-valued internal variable which represents the averaged isotropic resistance to macroscopic viscoplastic flow offered by the internal state of the polycrystalline material such as dislocation density, solid solution strengthening, subgrain and grain size effects. The particular forms of Eq. (34) which seem to be applicable to numerically simulate stress–viscoplastic strain behavior are those used to relate dislocation velocity with stress. In general, in those equations the dislocation velocity and, therefore, the equivalent viscoplastic strain rate are generally prescribed by power laws or exponential functions (Bodner and Partom, 1975; Miller, 1976; Nishiguchi et al., 1990).

Furthermore, experimental results on high-strength steels (Spitzig et al., 1975, 1976) showed that the equivalent stress c may be adequately described by the relation:

$$c = aI_1 + \sqrt{J_2}, \tag{35}$$

where a represents the hydrostatic stress coefficient. The coefficients, a and c, are strain-dependent, whereas experimental data have shown that the ratio $\alpha = a/c$ is constant. Thus, the equivalent stress (35) could alternatively be written in the form:

$$c = \frac{1}{1 - \alpha I_1} \sqrt{J_2}. \tag{36}$$

Now, using the rate formulation of Eq. (36)

$$\dot{c} = \frac{1}{1 - \alpha I_1} \left(\frac{1}{2\sqrt{J_2}} \mathrm{dev}\, \mathbf{T} + a\mathbf{1} \right) \cdot \dot{\mathbf{T}} \tag{37}$$

as well as Eqs. (29), (24) and (11), one arrives at the following scalar-valued rate constitutive equation

$$(1 - \alpha I_1)\dot{c} = \sqrt{2}\mu \dot{\epsilon}_{\mathrm{iso}} + 3aK\dot{\epsilon}_{\mathrm{vol}} - \left(\sqrt{2}\mu + 9\sqrt{2}abK \right) \dot{\gamma}_{\mathrm{iso}} \tag{38}$$

with the equivalent total isochoric and volumetric strain rates

$$\dot{\epsilon}_{\mathrm{iso}} = \mathbf{N} \cdot \mathrm{dev}\, \dot{\mathbf{H}} \tag{39}$$

and

$$\dot{\epsilon}_{\mathrm{vol}} = \mathrm{tr}\, \dot{\mathbf{H}}, \tag{40}$$

respectively.

4. Integration of the constitutive rate equations

A key factor in the computation of elastic–viscoplastic solids by the finite-element method is the numerical integration of the nonlinear constitutive equations governing the flow behavior and the evolution of internal state variables. In general, efficient and stable iterative techniques are employed to solve the discretized equilibrium equations for each time step in displacement-based finite-element procedures for nonlinear problems. The results of each iteration may be seen as estimates of the incremental displacements which are used to compute the current stress state and other field variables in the integration points of the finite elements. Accordingly, these variables are known at time t as well as the estimate of the total metric transformation tensor $\mathbf{Q}$ at time $t + \Delta t$. Then, the problem is to integrate the evolution equations for $\mathbf{Q}^{\mathrm{vp}}$ and c across the time increment Δt in order to calculate the current values of the stress and strain tensors.

Therefore, numerous researchers have proposed a number of integration algorithms which are based on explicit and implicit integration schemes. In particular, algorithms based on forward gradient methods have been developed, for example, by Zienkiewicz and Cormeau (1974) who approximated the nonlinear stress–strain relation by a tangent at the beginning of the time step. However, these algorithms are known to be limited in their step size in order to obtain satisfactory results. Cormeau (1975) has shown that with an explicit Euler forward time integration procedure the size of the time increment is generally restricted by numerical stability requirements. Unconditionally stable algorithms, on the other hand, are limited by the accuracy of the numerical results. The main advantage of using explicit integration schemes is the ease of implementation as they do not require the assembly and inversion of Jacobian matrices which can be of great advantage and significance especially when the number of equations involved is large. These advantages, however, are generally offset by the need of an excessive number of solution increments when a large elastic–viscoplastic strain analysis is performed. Zirky (1994) and Arya (1996) have discussed explicit integration algorithms involving generalized and higher-order Runge–Kutta methods which lead to considerable saving in computer time without adversely affecting the accuracy of the results.

To overcome the stability-related time increment restrictions Argyris et al. (1978) and Peirce et al. (1984), e.g., proposed semi-implicit time integration schemes based on linearized Taylor series expansions of the relevant constitutive functions. These algorithms allow much larger time increments without encountering stability problems or requiring iterations at the constitutive level. However, their algorithms become inaccurate and unstable if large time increments are taken during a period of sharp changes in stress–strain response.

Alternatively, in order to achieve accurate solutions for large time increments, taking into account the entire nonlinear structure of the constitutive equations, it is possible to solve these iteratively at the end of the time step. Such an accurate and stable algorithm is the well-known backward Euler scheme which may be seen as a generalization of the radial return technique of classical rate-independent plasticity proposed by Wilkins (1964). It leads to an implicit time-integration scheme based on the elastic predictor-plastic corrector algorithm often used in computational viscoplasticity (Taylor and Becker, 1983; Lush et al., 1989; Weber and Anand, 1990; Müller-Hoeppe and Wriggers, 1992; Zabaras and Arif, 1992; Auricchio and Taylor, 1994; Sansour and Kollmann, 1997; Rouainia and Perić, 1998).

Moreover, an alternative technique has initially been proposed by Nemat-Nasser and Chung (1992) and subsequently extended by Nemat-Nasser and Li (1992) and Fotiu and Nemat-Nasser (1996) who use a viscoplastic predictor followed by an elastic corrector step. They have shown that even for large time steps or for stiff equations such a viscoplastic predictor increment is already very close to the exact solution, and it suffices only to use one correction step to obtain accurate numerical results. This correction term can be derived as a function of known quantities and the algorithm becomes therefore explicit. In addition, Brünig et al. (1995) and Brünig (1996, 1999a,c) employed a generalized version of this plastic predictor technique within their rate-independent finite element analyses to solve large strain elastic–plastic problems. This

stable, accurate and efficient integration algorithm will now be extended to take into account rate-dependent material behavior.

In particular, the numerical integration of Eq. (38) during the interval $t \leqslant \Theta \leqslant t + \Delta t$ leads to

$$(1 - \alpha I_1^*)[c(t + \Delta t) - c(t)] = \sqrt{2}\mu(\Delta\epsilon - \Delta\gamma), \tag{41}$$

where I_1^* denotes the mean value of the first stress invariant over the given time interval, and the increment of the uniaxial strain is given by

$$\Delta\epsilon = \Delta\epsilon_{\text{iso}} + \frac{3aK}{\sqrt{2}\mu}\Delta\epsilon_{\text{vol}} \tag{42}$$

with its respective isochoric

$$\Delta\epsilon_{\text{iso}} = \int_t^{t+\Delta t} \mathbf{N} \cdot \dot{\mathbf{H}}\, \mathrm{d}\Theta \tag{43}$$

and volumetric parts

$$\Delta\epsilon_{\text{vol}} = \int_t^{t+\Delta t} \mathbf{1} \cdot \dot{\mathbf{H}}\, \mathrm{d}\Theta, \tag{44}$$

whereas the increment of the equivalent viscoplastic strain can be expressed in the form:

$$\Delta\gamma = \left(1 + \frac{9abK}{\mu}\right)\Delta\gamma_{\text{iso}}. \tag{45}$$

In the viscoplastic predictor step, the entire deformation increment is taken to be viscoplastic

$$\Delta\gamma_p = \Delta\epsilon \tag{46}$$

and, following Nemat-Nasser and Li (1992), the associated predictor equivalent stress at the end of the interval is estimated from the one-dimensional constitutive relationship

$$c_p(t + \Delta t) = c(\gamma(t) + \Delta\epsilon, \dot{\epsilon}). \tag{47}$$

Clearly, this leads to an overestimation of both the viscoplastic strain increment and the current equivalent stress measure. The respective errors are given by

$$\Delta_{\text{er}}c = c_p(t + \Delta t) - c(t + \Delta t), \tag{48}$$

$$\dot{\gamma}_{\text{er}}(\Theta) = \dot{\epsilon}(\Theta) - \dot{\gamma}(\Theta) = \frac{1 - \alpha I_1^*}{\sqrt{2}\mu}\dot{c}(\Theta), \tag{49}$$

and

$$\Delta_{\text{er}}\gamma = \dot{\gamma}_{\text{er}}^*\Delta t, \tag{50}$$

where $\dot{\gamma}_{\text{er}}^*$ is the mean value of $\dot{\gamma}_{\text{er}}(\Theta)$ over the time interval $t \leqslant \Theta \leqslant t + \Delta t$. Furthermore, it is assumed that the errors in the equivalent stress and equivalent viscoplastic strain are related by the constitutive relationship:

$$\Delta_{\text{er}}c \cong \frac{\partial c}{\partial\gamma}\Delta_{\text{er}}\gamma + \frac{\partial c}{\partial\dot{\gamma}}\dot{\gamma}_{\text{er}}^*, \tag{51}$$

where the differentials $\partial c/\partial\gamma$ and $\partial c/\partial\dot{\gamma}$ are computed at the end of the viscoplastic predictor increment. Now, using Eqs. (41), (48), (49) and (51) one obtains the following estimate of the error in the effective viscoplastic strain rate

$$\dot{\gamma}^*_{\mathrm{er}} = \frac{1}{\Delta t}\left[\frac{\sqrt{2}\mu}{1-\alpha I_1^*} + \frac{\partial c}{\partial \gamma} + \frac{1}{\Delta t}\frac{\partial c}{\partial \dot{\gamma}}\right]^{-1}(c_p(t+\Delta t) - c(t)), \tag{52}$$

and then the respective total viscoplastic strain and equivalent stress at the end of the time increment are given by

$$\gamma(t+\Delta t) = \gamma(t) + \Delta\gamma \tag{53}$$

with

$$\Delta\gamma = \Delta\gamma_{\mathrm{p}} - \dot{\gamma}^*_{\mathrm{er}}\Delta t, \tag{54}$$

$$c(t+\Delta t) = c(t) + \frac{\sqrt{2}\mu}{1-\alpha I_1^*}\dot{\gamma}^*_{\mathrm{er}}\Delta t. \tag{55}$$

Within this integration algorithm, the viscoplastic strain increment $\Delta\gamma$ must be positive in continuing viscoplastic flow. As pointed out by Nemat-Nasser and Chung (1992), $\Delta\gamma$ may become negative when the initial material response is essentially elastic and the time increments are very small. In this case, the current equivalent stress is approximated by

$$c(t+\Delta t) \cong c(t) + \frac{\sqrt{2}\mu}{1-\alpha I_1^*}\Delta\gamma_{\mathrm{p}}. \tag{56}$$

Moreover, the isochoric part of the equivalent viscoplastic strain increment is given by

$$\Delta\gamma_{\mathrm{iso}} = \left(1 + \frac{9abK}{\mu}\right)^{-1}\Delta\gamma. \tag{57}$$

Corresponding estimates of the respective tensorial quantities may now be derived using the above fundamental relationships. In particular, the incremental viscoplastic strain tensor is given by

$$\Delta\mathbf{H}^{\mathrm{vp}} = \mathrm{dev}\,\Delta\mathbf{H}^{\mathrm{vp}} + \tfrac{1}{3}\mathrm{tr}\,\Delta\mathbf{H}^{\mathrm{vp}}\mathbf{1}, \tag{58}$$

where

$$\mathrm{dev}\,\Delta\mathbf{H}^{\mathrm{vp}} = \Delta\gamma_{\mathrm{iso}}\hat{\mathbf{N}} \tag{59}$$

represents the deviator of the incremental viscoplastic strain tensor and the incremental inelastic dilatation may be computed from

$$\mathrm{tr}\,\Delta\mathbf{H}^{\mathrm{vp}} = 3\sqrt{2}b\,\Delta\gamma_{\mathrm{iso}}. \tag{60}$$

In Eq. (59), $\hat{\mathbf{N}}$ denotes the mean deviatoric orientation tensor (normalized deviatoric stress tensor) given by

$$\hat{\mathbf{N}} = \tfrac{1}{2}(\mathbf{N}(t+\Delta t) + \mathbf{N}(t)). \tag{61}$$

Taking into account the incremental elastic law,

$$\mathrm{dev}\,\Delta\mathbf{T} = \mathrm{dev}\,\mathbf{T}(t+\Delta t) - \mathrm{dev}\,\mathbf{T}(t) = 2\mu\,\mathrm{dev}\,(\Delta\mathbf{H}^{\mathrm{el}}) = 2\mu(\mathrm{dev}\,\Delta\mathbf{H} - \mathrm{dev}\,\Delta\mathbf{H}^{\mathrm{vp}}) \tag{62}$$

and making use of Eqs. (47), (48) and (39), the current unit normal

$$\mathbf{N}(t+\Delta t) = \frac{(\sqrt{2J_2(t)} - \mu\Delta\gamma_{\mathrm{iso}})\mathbf{N}(t) + 2\mu\,\mathrm{dev}\,(\Delta\mathbf{H})}{\sqrt{2J_2(t+\Delta t)} + \mu\Delta\gamma_{\mathrm{iso}}} \tag{63}$$

is also known. Therefore, all tensorial quantities can now be computed without any iteration. In particular, the elastic strain increment,

$$\Delta\mathbf{H}^{\mathrm{el}} = \Delta\mathbf{H} - \Delta\mathbf{H}^{\mathrm{vp}} = \frac{1}{2}\int_{t}^{t+\Delta t} (\ln \mathbf{Q}^{\mathrm{el}})^{\cdot} \mathrm{d}\Theta, \tag{64}$$

leads to the logarithm of the current elastic metric transformation tensor:

$$\ln \mathbf{Q}^{\mathrm{el}}(t+\Delta t) = \ln \mathbf{Q}^{\mathrm{el}}(t) + 2\,\Delta\mathbf{H}^{\mathrm{el}}. \tag{65}$$

Using Eq. (65), the current elastic logarithmic strain tensor (8) is then calculated by

$$\mathbf{H}^{\mathrm{el}}(t+\Delta t) = \tfrac{1}{2}\ln \mathbf{Q}^{\mathrm{el}}(t+\Delta t) = \mathbf{H}^{\mathrm{el}}(t) + \Delta\mathbf{H}^{\mathrm{el}}. \tag{66}$$

Finally, the respective current stress tensor $\mathbf{T}(t+\Delta t)$ follows from the hyperelastic constitutive relationship (24), while Eq. (25) yields the associated tensor of current elastic moduli $\mathbb{C}(t+\Delta t)$.

The current plastic metric transformation tensor may then be computed from

$$\mathbf{Q}^{\mathrm{vp}}(t+\Delta t) = \mathbf{Q}(t+\Delta t)\mathbf{Q}^{\mathrm{el}-1}(t+\Delta t), \tag{67}$$

where the elastic metric transformation is given by

$$\mathbf{Q}^{\mathrm{el}}(t+\Delta t) = \exp(2\mathbf{H}^{\mathrm{el}}). \tag{68}$$

5. Analysis of viscoplastic flow localization

Localization of deformation into narrow bands of intense straining is a characteristic feature of ductile metals when the fundamental smoothly varying inelastic deformations have reached a certain critical level. Once these bands form, they persist and the strains inside them can become very large without contributing much to the overall deformation of the body. This can lead to shear fracture at an overall strain only slightly larger than that at the onset of localization. These phenomena are often associated with a significant reduction of load-carrying capacity and, therefore, the onset of localization is naturally considered as the point of threshold to predict fracture of engineering structures. Over the last years considerable effort has been devoted to obtain a comprehensive understanding of the problem and to analyze the behavior quantitatively. It is well known that for classical elastic-isochorically plastic solids described via a smooth J_2 yield surface and normality of the plastic flow rule, no localization into shear bands is predicted at a realistic level of strains unless the strain hardening level is very low, but deviations from this classical model can have a strong destabilizing effect. In fact, the critical strain is considerably lowered by the assumption of hydrostatic stress-dependent theories of metals and non-normality of the plastic flow rule as proposed by Brünig (1999c). On the other hand, Needleman and Tvergaard (1984) studied the influence of strain rate on localization prediction, and it has been found that localization is significantly delayed by the increasing material strain rate sensitivity.

Theoretically, for rate-independent solids localization is associated with loss of ellipticity of the equations governing incremental equilibrium. Furthermore, finite-element solutions exhibit an inherent mesh dependence, and the minimum width of the band of localized deformation is given by the mesh spacing. Hence, key features of the numerical solutions can be a consequence of the finite-element discretization. This is clearly an undesirable state of affairs and stems from the character of the continuum equations. In addition, numerous attempts to simulate the localization behavior based on classical inelastic theories have been shown to be unsatisfactory because they are not able to describe softening after the onset of localization. This inability arises from the fact that classical theories do not contain any information about the size of the localization zone and, therefore, a length scale has to be implemented. This length scale should reflect the ability of the microstructure to transmit information to neighboring points within a certain distance between dislocations and grains. Thus, the length scale may be seen as a material property linking

the microstructure to the continuum. To overcome the problems of loss in ellipticity in the governing rate-independent equations or finite-element mesh dependencies of the narrow bands generalized continuum theories including internal length scales have been proposed. In particular, Mühlhaus and Aifantis (1991) and de Borst and Pamin (1996) among others discussed gradient-dependent plasticity theories, Bazant and Lin (1988) used nonlocal descriptions, whereas Mühlhaus (1989) employed a Cosserat continuum approach. On the other hand, the inelastic response of materials may be inevitably rate dependent. It has been shown by Needleman (1988) that rate-dependent theories implicitly introduce an internal length scale into the governing equations and, therefore, viscoplastic models like that discussed in this paper are well suited for analysing localization behavior of solids. In this case, the incremental equilibrium equations for quasi-static problems remain elliptic as long as stress levels remain small compared to elastic stiffness and, therefore, localization bifurcation is effectively excluded. The material rate dependence implicitly introduces a length scale into the governing equations although the constitutive description does not contain a material parameter with the dimension of length. This is essential in setting the shear band thickness and in giving a unique direction of the shear band as has been demonstrated by Wang et al. (1996). They showed that in viscoplastic models the material length scale equals the width of the shear band in the finite-element solutions. Therefore, the pathological mesh sensitivity associated with numerical solutions of localization problems for rate-independent materials is eliminated.

Fundamentals of the analysis of localization in elastic–plastic solids have been developed by Hill (1962) and Rice (1977). Briefly, the conditions of compatibility inside and outside the localized band, rate equilibrium across the band interfaces as well as associated constitutive relations lead to the fundamental equation governing the localization process, see Brünig (1996) for details. Its nontrivial solution determines the onset of localization, whereas the initial band orientations are computed using the eigenvalues of the corresponding acoustic tensor. This local analysis is performed at all integration points of the finite elements, whereas the subsequent development of the localized deformation pattern is obtained from a global numerical analysis described in the following section.

6. Computational aspects and finite-element implementation

To compute the components of the mixed-variant logarithmic strain tensor $\mathbf{H} = 1/2 \ln \mathbf{Q}$ in Eq. (2), Brünig (1999a) proposed the use of first and higher-order Padé approximations. In particular, taking account of the abbreviation,

$$\mathbf{A} = (\mathbf{Q} - \mathbf{1})(\mathbf{Q} + \mathbf{1})^{-1}, \tag{69}$$

it is possible to express the first Padé approximation of $\mathbf{H}$ by

$$\mathbf{H}_{(1)} = \mathbf{A}, \tag{70}$$

the second Padé approximation by

$$\mathbf{H}_{(2)} = \mathbf{A}(\mathbf{1} - \tfrac{1}{3}\mathbf{A}^2)^{-1}, \tag{71}$$

the third Padé approximation by

$$\mathbf{H}_{(3)} = (\mathbf{A} - \tfrac{4}{15}\mathbf{A}^3)(\mathbf{1} - \tfrac{3}{5}\mathbf{A}^2)^{-1}, \tag{72}$$

and the fourth Padé approximation by

$$\mathbf{H}_{(4)} = (\mathbf{A} - \tfrac{11}{21}\mathbf{A}^3)(\mathbf{1} - \tfrac{6}{7}\mathbf{A}^2 + \tfrac{3}{35}\mathbf{A}^4)^{-1}, \tag{73}$$

respectively. In a large number of numerical simulations, the first Padé approximation (70) is an excellent approximation of the true value of the logarithm as long as the principal metric tensor components remain

moderate. But for larger principal stretches, the use of higher-order Padé approximations is necessary to compute the components of the Hencky strain tensor in an accurate manner. Limits for the application of the respective Padé approximations (70)–(73) have been examined in some detail by Brünig (1999a,b). The materials considered in this paper are characterized by small elastic strains compared to the total strains. Therefore, the elastic strain tensor is accurately computed by the first Padé approximation, whereas the total strain components may require higher-order Padé approximations. Similarly, the elastic tensor exponent $\mathbf{Q}^{\mathrm{el}}(t+\Delta t)=\exp(2\ \mathbf{H}^{\mathrm{el}})$ in Eq. (68) will be determined by the first Padé approximation:

$$\mathbf{Q}^{\mathrm{el}}_{(1)}=(\mathbf{1}-\mathbf{H}^{\mathrm{el}})^{-1}(\mathbf{1}+\mathbf{H}^{\mathrm{el}}), \tag{74}$$

which leads to a sufficiently accurate value of the elastic exponential function.

Furthermore, in order to preserve the convergence in the iterative solution algorithm the above constitutive technique is employed in conjunction with the consistent current tensor of elastic–viscoplastic moduli:

$$\mathbb{C}^{\mathrm{ev}}=\frac{\mathrm{d}\mathbf{T}}{\mathrm{d}\mathbf{H}}. \tag{75}$$

In particular, taking into account the current tensor of elastic moduli (25), the differential formulation of Eq. (24) is given by

$$\mathrm{d}\mathbf{T}=\mathbb{C}\,\mathrm{d}\mathbf{H}^{\mathrm{el}}, \tag{76}$$

where – using integration of Eq. (11) as well as Eq. (66) – the differential of the elastic strain tensor is obtained from

$$\mathrm{d}\mathbf{H}^{\mathrm{el}}=\mathrm{d}\Delta\mathbf{H}^{\mathrm{el}}=\mathrm{d}\Delta\mathbf{H}-\mathrm{d}\Delta\mathbf{H}^{\mathrm{vp}} \tag{77}$$

and with Eqs. (56)–(58) one gets

$$\mathrm{d}\Delta\mathbf{H}^{\mathrm{vp}}=(\hat{\mathbf{N}}+\sqrt{2}b\mathbf{1})\mathrm{d}\Delta\gamma_{\mathrm{iso}}+\tfrac{1}{2}\Delta\gamma_{\mathrm{iso}}\,\mathrm{d}\mathbf{N}, \tag{78}$$

$$\mathrm{d}\Delta\gamma_{\mathrm{iso}}=\left(1+\frac{9abK}{\mu}\right)^{-1}\mathrm{d}\Delta\gamma. \tag{79}$$

Furthermore, Eqs. (41), (44), (46), (51) and (52) lead to the differential of the scalar valued viscoplastic strain increment

$$\mathrm{d}\Delta\gamma=\frac{\sqrt{2}\mu}{\sqrt{2}\mu+(1-\alpha I_1)(\frac{\partial c}{\partial\gamma}+\frac{1}{\Delta t}\frac{\partial c}{\partial\dot{\gamma}})}(\mathrm{d}\mathbf{N}\cdot\Delta\mathbf{H}+\mathbf{N}\cdot\mathrm{d}\Delta\mathbf{H})+\frac{3aK}{\sqrt{2}\mu+(1-\alpha I_1)(\frac{\partial c}{\partial\gamma}+\frac{1}{\Delta t}\frac{\partial c}{\partial\dot{\gamma}})}\mathbf{1}\cdot\mathrm{d}\Delta\mathbf{H}. \tag{80}$$

In addition, Eq. (29) yields

$$\mathrm{d}\mathbf{N}=\frac{-1}{\sqrt{2}J_2}\mathrm{dev}\,\mathbf{T}\,\mathrm{d}\sqrt{J_2}+\frac{1}{\sqrt{2J_2}}\mathrm{d}\,(\mathrm{dev}\,\mathbf{T}) \tag{81}$$

with

$$\mathrm{d}\sqrt{J_2}=\frac{1}{\sqrt{2}}\mathbf{N}\cdot\mathrm{d}\mathbf{T}. \tag{82}$$

Substituting Eq. (82) into Eq. (81) then leads to

$$\mathrm{d}\mathbf{N}=\frac{-1}{\sqrt{2J_2}}(\mathbf{N}\otimes\mathbf{N})\,\mathrm{d}\mathbf{T}+\frac{1}{\sqrt{2J_2}}\mathbb{1}^{D}\,\mathrm{d}\mathbf{T}, \tag{83}$$

where $\mathbb{1}^D$ is given by Eq. (26). Finally, Eqs. (76)–(83) furnish the following tensorial representation of the algorithmic elastic–viscoplastic moduli:

$$\mathbb{C}^{\mathrm{ev}} = \left[\mathbb{1} + \frac{\mu\Delta\gamma}{\sqrt{2J_2}}(\mathbb{1}^D - \mathbf{N}\otimes\mathbf{N})\right]^{-1}\left[\mathbb{C} - \left(1 + \frac{9abK}{\mu}\right)^{-1}\frac{1}{\sqrt{2}\mu + (1-\alpha I_1)(\frac{\partial c}{\partial\gamma} + \frac{1}{\Delta t}\frac{\partial c}{\partial\dot{\gamma}})}\right.$$
$$\left.\times\,(2\sqrt{2}\mu^2\hat{\mathbf{N}}\otimes\mathbf{N} + 6aK\mu\hat{\mathbf{N}}\otimes\mathbf{1} + 6abK\mu\mathbf{1}\otimes\mathbf{N} + 9\sqrt{2}abK\mu\mathbf{1}\otimes\mathbf{1})\right]. \tag{84}$$

Following Brünig (1999a), the finite-element procedure is based on the principle of virtual work

$$\int_{B_0}\delta\mathbf{H}\cdot\mathbf{T}\,\mathrm{d}v_0 - \int_{\partial B_0}\delta\mathbf{u}\cdot\bar{\mathbf{t}}_0\,\mathrm{d}a_0 = 0, \tag{85}$$

where B_0 and ∂B_0 denote the volume and surface of the body in the initial configuration. The first integral in Eq. (85) represents the variation of the current stored energy density while the second accounts for the contribution of the prescribed surface tractions $\bar{\mathbf{t}}_0$.

Using a consistent linearization procedure, choosing suitable shape functions and nodal degrees of freedom for the unknown displacements, carrying out the integrations and finally assembling the individual element stiffness matrices and load vectors, one arrives – as usual – at a set of linearized algebraic equations for the nodal displacement increments, which may be written in the familiar abbreviated form:

$$\mathbf{K}_{\mathrm{T}}\Delta\mathbf{V} = \mathbf{R}. \tag{86}$$

In Eq. (86), $\mathbf{K}_{\mathrm{T}}$ denotes the global tangent stiffness matrix, $\mathbf{R}$ corresponds to the residual unbalanced force vector, and $\Delta\mathbf{V}$ represents the vector of incremental displacements. Eq. (86) is solved recursively and leads to a converged solution as long as the equations governing incremental equilibrium remain elliptic. Due to the rate dependence of the material behavior ellipticity is satisfied as long as stress levels remain small compared to elastic stiffness even after the onset of localization is computed in some Gaussian points of individual elements and, therefore, the formation of localized deformation modes can be simulated numerically.

7. Numerical simulations

7.1. Material properties

Following the ideas of Hutchinson (1976) and Pan and Rice (1983) describing the rate-dependent motion of dislocations on the microscale, the present macroscopic analysis employs the power-law nonlinear viscous form:

$$c(\gamma,\dot{\gamma}) = g(\gamma)\left(\frac{\dot{\gamma}}{\dot{\mu}}\right)^m \tag{87}$$

as an appropriate constitutive function in the rate-dependent model. In general, a power law description of material strain-rate sensitivity is not a fundamental microphysical relation, although it can provide a reasonable representation of the strain-rate sensitivity of common structural metals over several decades of strain rates. The physical background for power-law viscoplasticity and its limitations are, e.g. discussed by Asaro (1983) and, in addition, Pan and Rice (1983) have shown that Eq. (87) describes a fairly large range

of experimentally observed behavior of metal solids. In particular, the reference stress $g(\gamma)$ characterizes the current state of strain hardening of the polycrystalline metal as long as inelastic deformations occur, the reference inelastic strain rate $\dot{\mu}$ is defined in such a way that $\dot{\gamma}$ equals $\dot{\mu}$ whenever the effective stress measure c equals g, and m denotes the strain rate sensitivity parameter defined as $m = \partial(\ln c)/\partial(\ln \dot{\gamma})$.

The reference stress $g(\gamma)$ is found by fitting the numerical results of uniaxial tension and compression tests to experimental data. For example, Spitzig et al. (1975, 1976) presented experiments on iron-based materials, and their tests were conducted at small nominal strain rates of $\dot{\mu} = 2.0 \times 10^{-4}$ s^{-1} or $\dot{\mu} = 2.5 \times 10^{-4}$ s^{-1}. In particular, the current strength coefficient $g(\gamma)$ will be simulated numerically by the power law:

$$g = g_0 \left(\frac{H\gamma}{n g_0} \right)^n. \tag{88}$$

In Eq. (88), g_0 means the rate-independent reference stress, H represents the initial hardening parameter and n denotes the hardening exponent. This model does not contain any explicit yield stress but the equivalent stress–equivalent plastic strain relationship is such that in the small regime inelastic strains can be of insignificant magnitude and, therefore, quasi-elastic deformations are computed. Fig. 1 shows the current strength-equivalent plastic strain curve for 4330 steel. As can be seen, the chosen material properties $g_0 = 1020$ MPa, $H = 2900$ MPa, and $n = 0.075$ lead to good agreement with the experimental data presented by Spitzig et al. (1975).

Some iron-based materials, however, show strong saturation behavior. Thus, the current reference stress of aged maraging steel is assumed to be adequately described by the saturation law:

$$g = g_S \tanh \left(\frac{H\gamma}{g_S} \right), \tag{89}$$

where g_S denotes the saturation flow strength. The experimental data presented by Spitzig et al. (1976) are numerically simulated with $H = 700\,000$ MPa and $g_S = 1120$ MPa (Fig. 2).

In addition, experiments (Spitzig and Richmond, 1984) have shown that the flow stress depends nearly linearly on hydrostatic stress which will be described by the equivalent stress measure c (36) taking into account the hydrostatic stress coefficient α. As has been discussed by Brünig (1999c), the experimental data can be simulated numerically in an accurate manner with $\alpha = 20$ TPa^{-1}.

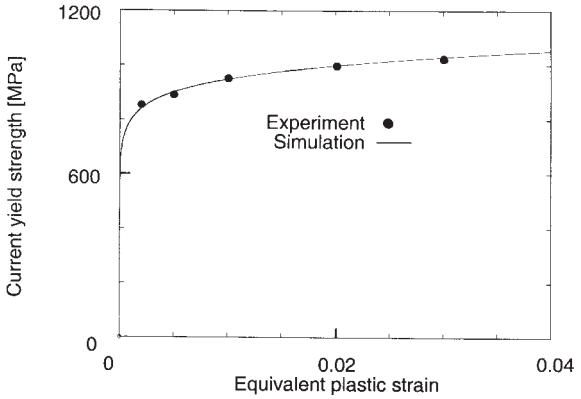

Fig. 1. Current yield strength-equivalent plastic strain curve for 4330 steel.

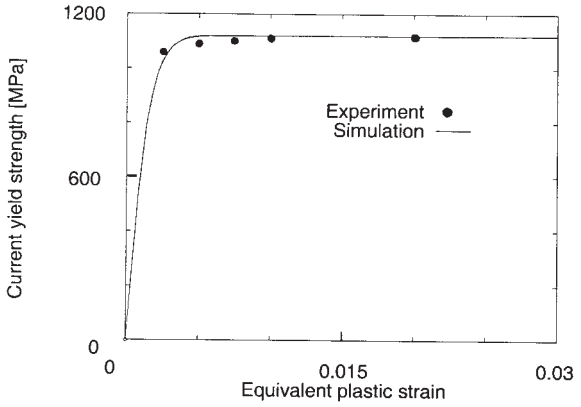

Fig. 2. Current yield strength-equivalent plastic strain curve for aged maraging steel.

Moreover, tension and compression tests with aged maraging steel as well as 4310 and 4330 steels – which were conducted over a small strain range with small strain rates – have shown irreversible volume expansions which are approximately proportional to the inelastic strain. The underlying physical process is assumed to be an increase in dislocation density as long as crystallographic deformations occur. Following Brünig (1999c), the increase in permanent volume expansion will be limited, and the kinematic parameter b appearing in the flow rule (31) is assumed to be nearly unaffected by rate effects, and, therefore, will be computed from the volumetric viscoplastic strain:

$$\gamma_{\mathrm{vol}} = \gamma_{\mathrm{vol,S}} \tanh(10\gamma). \tag{90}$$

The saturation values are assumed to be $\gamma_{\mathrm{vol,S}} = 4.8 \times 10^{-4}$ in aged maraging steel and $\gamma_{\mathrm{vol,S}} = 6.5 \times 10^{-4}$ in 4310 and 4330 steels.

7.2. Rectangular specimens with clamped straight ends

The numerical analyses discussed in this section deal with the finite deformation behavior and localization predictions of uniaxially loaded rectangular specimens with clamped straight ends. Numerical calculations take into account plane strain conditions and the finite element mesh of the bars with length $l = 4.0$ and width $h = 1.0$ is built up with 1600 crossed-triangle elements based on linear displacement fields. Note that due to the inhomogeneous boundary conditions, no geometrical imperfections are needed to obtain localized deformation modes. The elastic material behavior of steel is adequately described by Young modulus $E = 200\,000$ MPa and Poisson's ratio $\nu = 0.3$, whereas the viscoplastic material properties are simulated by the nonlinearly work-hardening models discussed above.

First, the elastic–viscoplastic deformation behavior of bars formed with aged maraging steel with rate-sensitivity parameter $m = 0.002$ will be studied in some detail. In particular, if the effective stress measure c is assumed to be described by the J_2 criterion ($\alpha = 0$ in Eq. (36)), the load-deflection curve given in Fig. 3 shows a maximum at the elongation $\bar{u}/l = 0.017$ and thereafter a remarkable decrease in load is observed which at final elongation $\bar{u}/l = 0.125$ remains about 35%. After the maximum in load has been passed smooth deformations occur, but at $\bar{u}/l = 0.073$ the onset of localization is predicted in the center region of the bar. However, if the effective stress measure c is described by the I_1–J_2 criterion (36) with $\alpha = 20$ TPa^{-1} (which is the material parameter for steels observed in the experiments discussed above) a similar load–deflection curve is obtained, but the load maximum is about 6% smaller. Then, shortly after the load maximum has been passed remarkably earlier onset of localization is predicted at $\bar{u}/l = 0.022$. Thus, nu-

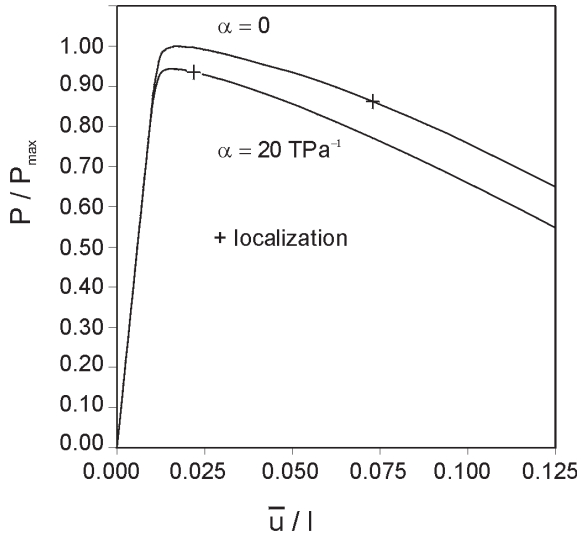

Fig. 3. Load-deflection curves based on $m = 0.002$ with various α.

merical calculations which take into account hydrostatic stress terms lead to smaller loads and to localization at remarkably smaller elongations. Therefore, hydrostatic stress sensitivity may lead to a notable decrease in ductility of metal specimens and should not be neglected in accurate localization predictions.

Furthermore, the influence of the rate sensitivity parameter m on the deformation and localization behavior of hydrostatic stress-sensitive steel bars ($\alpha = 20$ TPa^{-1}) is studied numerically in some detail. In particular, the strain rate sensitivity $m = 0.0005$ is chosen and this small value characterizes nearly rate-independent material behavior. As can be seen from Fig. 4, the load–deflection curve shows its maximum at 1.50% elongation and, afterwards, a remarkable decrease in load is observed which at the elongation $\bar{u}/l = 0.075$ is about 50%. Shortly after the load maximum has been passed the onset of localization is predicted at 1.75% elongation. Corresponding deformed configurations are shown in Fig. 5. Primary localization into shear bands occurs in the center region of the bar, and the corresponding inclination of the shear band angle is 43° with respect to the loading axis. Fig. 5 clearly shows that with increasing elongation shear bands occur which spread over moderately large areas.

In addition, Fig. 4 shows the load–deflection curve for $m = 0.002$ discussed above. This increase in material rate sensitivity leads to an increase in maximum load of only 1% as well as to an increase in elongation at the onset of localization of about 25% but to a remarkably smaller decrease in load-deflection curve. In particular, at $\bar{u}/l = 0.075$ the load is about 57% larger than in the case of $m = 0.0005$. Corresponding deformed configurations are shown in Fig. 6. Again, primary localization is computed in the center region of the bar and the associated inclination of the shear band angle is 43°. Then, with increasing elongation shear bands spread over remarkably wider areas, and the global deformation behavior is superposed by a neck.

As can also be seen from Fig. 4, further increases in material rate sensitivity lead to lower decreases in load after their maxima have been passed and the onset of localization is significantly delayed. In particular, for $m = 0.005$ the onset of localization is predicted at 6% elongation and the corresponding shear band inclination is 29° with respect to the loading axis. Corresponding deformed configurations given in Fig. 7 clearly demonstrate that further spread of shear bands during continuing elongation is largely prevented by the development of a dominant neck. Hence, superposed necking becomes more and more dominant when larger strain rate sensitivity parameters are considered. As can be seen from Fig. 4, the numerical

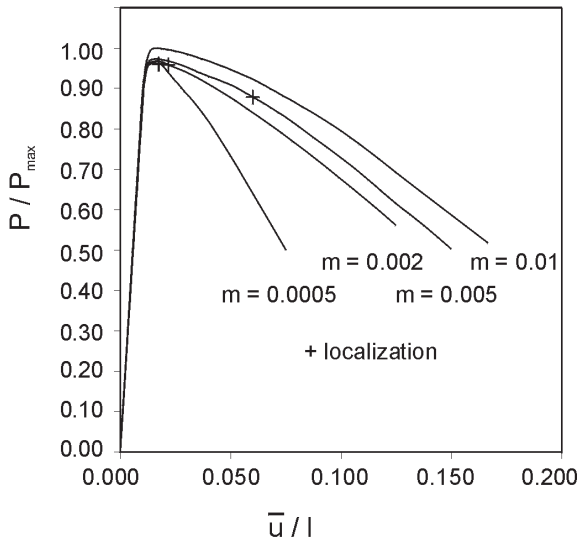

Fig. 4. Load-deflection curves based on $\alpha = 20\ \mathrm{TPa}^{-1}$ with various m.

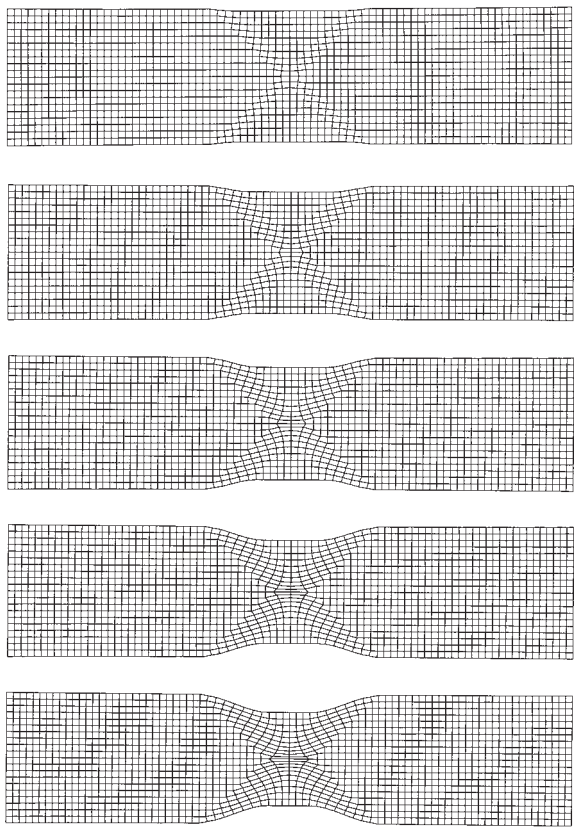

Fig. 5. Deformed configurations based on $m = 0.0005$ at $u/u_{\max} = 0.33$, 0.50, 0.67, 0.83, and 1.00.

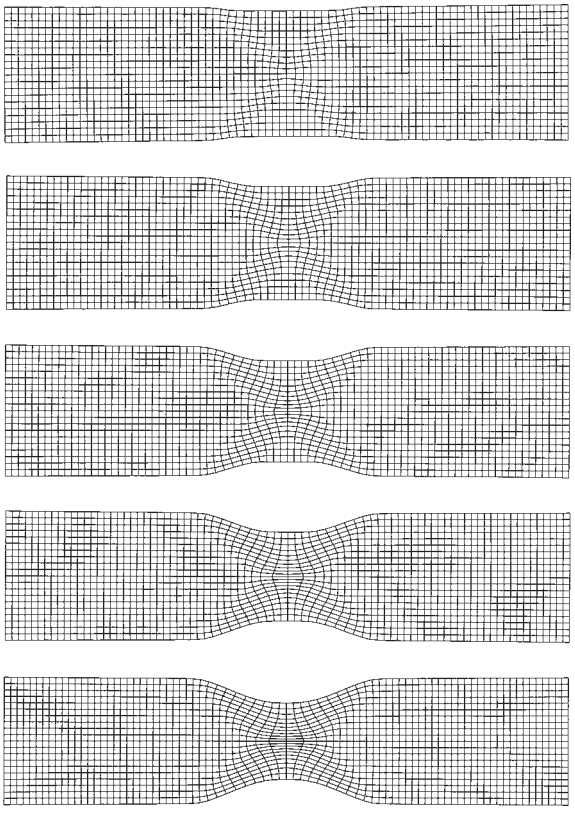

Fig. 6. Deformed configurations based on $m = 0.002$ at $u/u_{\max} = 0.33$, 0.50, 0.67, 0.83, and 1.00.

calculation based on $m = 0.01$ predicts about 5% greater load maximum and smooth elastic–viscoplastic deformation behavior when the load maximum has been passed without any localized shear band development at all.

8. Conclusions

A nonlinear finite element model for the macroscopic rate-dependent analysis of hydrostatic stress-sensitive metals has been presented. The continuum formulation is based on the multiplicative decomposition of the mixed-variant metric transformation tensor. This leads to the additive split of the rate of appropriate logarithmic strain tensors into elastic and viscoplastic as well as into isochoric and volumetric parts. Particular attention has been focused on the formulation of the generalized I_1–J_2 equivalent stress measure to be able to simulate numerically the effect of hydrostatic stress on the material properties in metals. Corresponding numerical aspects have been discussed in some detail.

The numerical calculations dealing with the finite deformation behavior of steel specimens undergoing tension tests have shown that the application of hydrostatic stress-sensitive and rate-dependent material models remarkably influence the prediction of the load–deflection behavior and the onset of localization. Furthermore, increasing strain rate sensitivity parameters have a notable effect on the subsequent localized

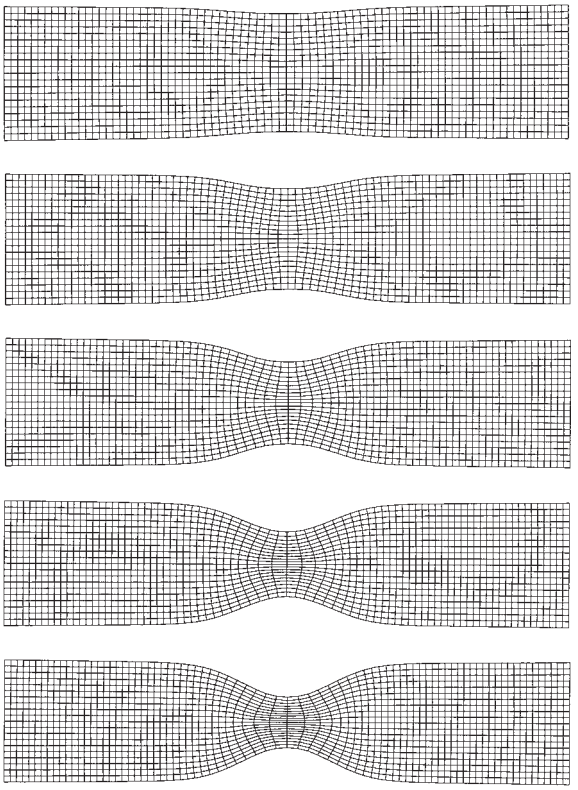

Fig. 7. Deformed configurations based on $m = 0.005$ at $u/u_{\max} = 0.33$, 0.50, 0.67, 0.83, and 1.00.

deformation modes. In particular, material models including small strain rate sensitivity predict that the onset of localization occurs at lower strain levels and lead to more distinct and smaller shear bands in uniaxial tests. By contrast, numerical calculations based on larger strain rate sensitivity parameters show the development of a (superposed) neck.

References

Anand, L., 1985. Constitutive equations for hot-working metals. Int. J. Plasticity 1, 213–231.

Arya, V.K., 1996. Efficient and accurate explicit integration algorithms with application to viscoplastic models. Int. J. Numer. Meth. Engng. 39, 261–279.

Argyris, J.H., Vaz, L.E., Willam, K.J., 1978. Improved solution methods for rate problems. Comp. Meth. Appl. Mech. Engng. 16, 231–277.

Asaro, R.J., 1983. Micromechanics of crystals and polycrystals. Adv. Appl. Mech. 23, 2–115.

Auricchio, F., Taylor, R.L., 1994. A generalized viscoplastic model and its algorithmic implementation. Comput. and Struct. 53, 637–647.

Bazant, Z.P., Lin, F.B., 1988. Non-local yield limit degradation. Int. J. Numer. Meth. Engng. 26, 1805–1823.

Bodner, S.R., Partom, Y., 1975. Constitutive equations for elastic–viscoplastic strain-hardening materials. J. Appl. Mech. 42, 385–389.

de Borst, R., Pamin, J., 1996. Some novel developments in finite element procedures for gradient-dependent plasticity. Int. J. Numer. Meth. Engng. 39, 2477–2505.

Brünig, M., 1996. Macroscopic theory and nonlinear finite element analysis of micromechanics of single crystals at finite strains. Comput. Mech. 18, 471–484.

Brünig, M., 1997. Numerical modelling of finite elastic-plastic deformations of crystalline solids including non-Schmid effects. In: Owen, D.R.J., Oñate, E., Hinton, E. (Eds.), Computational Plasticity 5 – Fundamentals and Applications, CIMNE, Barcelona, 907–912.

Brünig, M., 1998. Microscopic modelling of volume expansion and pressure dependence of plastic yielding in crystalline solids. Archive Appl. Mech. 68, 71–84.

Brünig, M., 1999a. Large strain elastic-plastic theory and nonlinear finite element analysis based on metric transformation tensors. Comput. Mech. 24, 187–196.

Brünig, M., 1999b. Formulation and numerical treatment of incompressibility constraints in large strain elastic–plastic analysis. Int. J. Numer. Meth. Engng. 45, 1047–1068.

Brünig, M., 1999c. Numerical simulation of the large elastic–plastic deformation behavior of hydrostatic stress-sensitive solids. Int. J. Plasticity 15, 1237–1264.

Brünig, M., Obrecht, H., 1998. Finite elastic–plastic deformation behavior of crystalline solids based on a non-associated macroscopic flow rule. Int. J. Plasticity 14, 1189–1208.

Brünig, M., Obrecht, H., Speier, L., 1995. Finite deformation elastic–plastic analysis based on a plastic predictor method. In: Owen, D.R.J., Oñate, E. (Eds.), Computational Plasticity 4 – Fundamentals and Applications, Pineridge Press, Swansea, 141–152.

Cormeau, I.C., 1975. Numerical stability of quasi-static elasto/visco-plasticity. Int. J. Numer. Meth. Engng. 9, 109–127.

Fotiu, P.A., Nemat-Nasser, S., 1996. A universal integration algorithm for rate-dependent elastoplasticity. Comput. and Struct. 59, 1173–1184.

Eterovic, A.L., Bathe, K.-J., 1990. A hyperelastic-based large strain elasto-plastic constitutive formulation with combined isotropic-kinematic hardening using logarithmic stress and strain measures. Int. J. Numer. Methods Eng. 30, 1099–1114.

Hill, R., 1950. The Mathematical Theory of Plasticity. Oxford University Press, Oxford.

Hill, R., 1962. Acceleration waves in solids. J. Mech. Phys. Solids 10, 1–16.

Hutchinson, J.W., 1976. Bounds and self-consistent estimates for creep of polycrystalline materials. Proc. R. Soc. Lond. A. 348, 101–127.

Khan, A.S., Huang, S., 1995. Continuum Theory of Plasticity. Wiley, New York.

Lee, E.H., 1969. Elastic–plastic deformations at finite strains. J. Appl. Mech. 36, 1–6.

Lehmann, Th., 1982a. Some remarks on the decomposition of deformations and mechanical work. Int. J. Eng. Sci. 20, 281–288.

Lehmann, Th., 1982b. Some theoretical considerations and experimental results concerning elastic–plastic stress–strain relations. Arch. Appl. Mech. (Ingenieur-Archiv) 52, 391–403.

Lush, A.M., Weber, G., Anand, L., 1989. An implicit time-integration procedure for a set of Internal variable constitutive equations for isotropic elasto-viscoplasticity. Int. J. Plasticity 5, 521–549.

Miller, A.K., 1976. An inelastic constitutive model for monotonic, cyclic and creep deformation. Part I. Equations development and analytical procedures. Trans. ASME J. Engng. Mater. Technol. 98, 106–113.

Mühlhaus, H.B., 1989. Application of Cosserat theory in numerical solutions of limit load problems. Archive Appl. Mech. (Ing.-Archiv) 59, 124–137.

Mühlhaus, H.B., Aifantis, E.C., 1991. A variational principle for gradient plasticity. Int. J. Solids Struct. 28, 845–857.

Müller-Hoeppe, N., Wriggers, P., 1992. Numerical integration of viscoplastic material laws at large strains with application to impact problems. Comput. and Struct. 45, 165–171.

Needleman, A., 1988. Material rate dependence and mesh sensitivity in localization problems. Comp. Meth. Appl. Mech. Engng. 67, 69–85.

Needleman, A., Tvergaard, V., 1984. Limits to formability in rate-sensitive metal sheets. In: Carlsson, J., Ohlson, N.G. (Eds.), Mechanical Behavior of Materials, Pergamon Press, Oxford, pp. 51–65.

Nemat-Nasser, S., Chung, D.T., 1992. An explicit constitutive algorithm for large-strain, large-strain-rate elastic-viscoplasticity. Comp. Meth. Appl. Mech. Engng. 95, 205–219.

Nemat-Nasser, S., Li, Y.F., 1992. A new explicit algorithm for finite-deformation elastoplasticity and elastoviscoplasticity: performance evaluation. Comput. and Struct. 44, 937–963.

Nishiguchi, I., Sham, T.-L., Krempl, E., 1990. A finite deformation theory of viscoplasticity based on overstress: part I – Constitutive equations. J. Appl. Mech. 57, 553–561.

Pan, J., Rice, J.R., 1983. Rate sensitivity of plastic flow and implications for yield-surface vertices. Int. J. Solids Struct. 19, 973–987.

Peirce, D., Shih, N., Needleman, A., 1984. A tangent modulus method for rate dependent solids. Comput. and Struct. 18, 875–887.

Perić, D., Owen, D.R.J., Honnor, M.E., 1992. A model for finite strain elasto-plasticity based on logarithmic strains: Computational issues. Comp. Meth. Appl. Mech. Engng. 94, 35–61.

Perzyna, P., 1966. Fundamental problems in viscoplasticity. Adv. Appl. Mech. 9, 243–377.

Rice, J.R., 1970. On the structure of stress-strain relations for time-dependent plastic deformations in metals. ASME J. Appl. Mech. 37, 728–737.

Rice, J.R., 1971. Inelastic constitutive relations for solids: An Internal variable theory and its applications to metal plasticity. J. Mech. Phys. Solids 19, 433–455.

Rice, J.R., 1977. The localization of plastic deformation. In: Koiter, W.T. (Ed.), Proc., 14th Int. Congr. Theoret. Appl. Mech., North-Holland, Amsterdam, pp. 207–220.

Rouainia, M., Perić, D., 1998. A computational model for elasto-viscoplastic solids at finite strain with reference to thin shell applications. Int. J. Numer. Meth. Engng. 42, 289–311.

Sansour, C., Kollmann, F.G., 1997. On theory and numerics of large viscoplastic deformation. Comput. Meth. Appl. Mech. Engng. 146, 351–369.

Spitzig, W.A., Richmond, O., 1984. The effect of pressure on the flow stress of metals. Acta Metall. 32, 457–463.

Spitzig, W.A., Sober, R.J., Richmond, O., 1975. Pressure dependence of yielding and associated volume expansion in tempered martensite. Acta Metall. 23, 885–893.

Spitzig, W.A., Sober, R.J., Richmond, O., 1976. The effect of hydrostatic pressure on the deformation behavior of maraging and HY-80 steels and its implications for plasticity theory. Metall. Trans. A 7A, 1703–1710.

Taylor, L.M., Becker, E.B., 1983. Some computational aspects of large deformation, rate-dependent plasticity problems. Comput. Meth. Appl. Mech. Engng. 41, 251–277.

Wang, W.M., Sluys, L.J., Borst, R., 1996. Interaction between material length scale and imperfection size for localization phenomena in viscoplastic media. Eur. J. Mech. A Solids 15, 447–464.

Weber, G., Anand, L., 1990. Finite deformation constitutive equations and a time integration procedure for isotropic, hyperelastic–viscoplastic solids. Comput. Meth. Appl. Mech. Engng. 79, 173–202.

Wilkins, M.L., 1964. Calculation of elastic–plastic flow. In: Alder, B. et al. (Eds.), Meth. Comp. Physics, vol. 3. Academic Press, New York.

Zabaras, N., Arif, F.M., 1992. A family of integration algorithms for constitutive equations in finite deformation elasto-viscoplasticity. Int. J. Numer. Meth. Engng. 33, 59–84.

Zienkiewicz, O.C., Cormeau, I.C., 1974. Viscoplasticity, plasticity and creep in elastic solids – a unified numerical solution approach. Int. J. Numer. Meth. Engng. 8, 821–845.

Zirky, M.A., 1994. An accurate and stable algorithm for high strain-rate finite strain plasticity. Comput. and Struct. 50, 337–350.